



# In vivo imaging of synaptic SV2A protein density in healthy and striatal-lesioned rats with [<sup>11</sup>C]UCB-J PET

Majken B Thomsen<sup>1,2</sup>, Jan Jacobsen<sup>1</sup>, Thea P Lillethorup<sup>1</sup> , Anna C Schacht<sup>1</sup>, Mette Simonsen<sup>1</sup>, Marina Romero-Ramos<sup>2</sup>, David J Brooks<sup>1,3</sup> and Anne M Landau<sup>1,4</sup> 

## Abstract

The number of functionally active synapses provides a measure of neural integrity, with reductions observed in neurodegenerative disorders. [<sup>11</sup>C]UCB-J binds to synaptic vesicle 2A (SV2A) transmembrane protein located in secretory vesicles. We aimed to assess [<sup>11</sup>C]UCB-J PET as an in vivo biomarker of regional cerebral synaptic SV2A density in rat lesion models of neurodegeneration. Healthy anesthetized rats had [<sup>11</sup>C]UCB-J PET and arterial blood sampling. We compared different models describing [<sup>11</sup>C]UCB-J brain uptake kinetics to determine its regional distribution. Blocking studies were performed with levetiracetam (LEV), an antiepileptic SV2A antagonist. Tracer binding was measured in rodent unilateral acute lesion models of Parkinsonism and Huntington's disease, induced with 6-hydroxydopamine (6-OHDA) and quinolinic acid (QA), respectively. [<sup>3</sup>H]UCB-J autoradiography was performed in postmortem tissue. Rat brain showed high and fast [<sup>11</sup>C]UCB-J uptake and washout with up to 80% blockade by LEV. [<sup>11</sup>C]UCB-J PET showed a 6.2% decrease in ipsilateral striatal SV2A binding after 6-OHDA and 39.3% and 55.1% decreases after moderate and high dose QA confirmed by autoradiography. In conclusion, [<sup>11</sup>C]UCB-J PET provides a good in vivo marker of synaptic SV2A density which can potentially be followed longitudinally along with synaptic responses to putative neuroprotective agents in models of neurodegeneration.

## Keywords

[<sup>11</sup>C]UCB-J PET, SV2A protein, neurodegeneration, synapse, rat

Received 29 January 2020; Revised 30 April 2020; Accepted 5 May 2020

## Introduction

The chemical synapse is the major locus for direct communication between neurons. The presynaptic terminal contains vesicles with neurotransmitters that can be released into the synaptic cleft, act on postsynaptic receptors and then be taken up by terminal and vesicle transporters which play an essential role in synaptic plasticity. Presynaptic dysfunction occurs in neurodegenerative diseases including Parkinson's,<sup>1</sup> Alzheimer's<sup>2</sup> and Huntington's disease<sup>3</sup> causing both impaired motor and cognitive function.

The recently developed PET tracer [<sup>11</sup>C]UCB-J binds to the synaptic vesicle glycoprotein 2A (SV2A), a transmembrane protein expressed ubiquitously and located in presynaptic vesicles throughout the brain.<sup>4,5</sup> SV2A plays an important role in synaptic

<sup>1</sup>Department of Nuclear Medicine and PET Center, Department of Clinical Medicine, Aarhus University, Aarhus, Denmark

<sup>2</sup>Department of Biomedicine, Aarhus University, Aarhus, Denmark

<sup>3</sup>Translational and Clinical Research Institute, Newcastle upon Tyne University, Newcastle upon Tyne, UK

<sup>4</sup>Translational Neuropsychiatry Unit, Department of Clinical Medicine, Aarhus University, Aarhus, Denmark

## Corresponding author:

Anne M Landau, Department of Nuclear Medicine and PET Center and Translational Neuropsychiatry Unit, Department of Clinical Medicine, Aarhus University, Palle Juul-Jensens Boulevard 165, J320, Aarhus N 8200, Denmark.

Email: [alandau@clin.au.dk](mailto:alandau@clin.au.dk)

vesicle function and [11C]UCB-J PET has been suggested to provide an *in vivo* marker of synaptic density and presynaptic integrity. Earlier studies of synaptic density have relied on postmortem methods where biopsies were used to quantify the synapses using synaptophysin histology, electron microscopy or Western blotting.<sup>6</sup> The use of [11C]UCB-J PET allows the *in vivo* study of synaptic SV2A density in living individuals that can be applied when diagnosing active disease and monitoring progression.

The cerebral uptake and binding properties of [11C]UCB-J have been investigated in monkeys, humans and mice,<sup>4,7–10</sup> where after intravenous injection it was found to enter the brain with a high extraction, fast uptake and washout kinetics and showed an acceptable rate of systemic metabolism. It revealed specific binding to SV2A protein in grey matter regions and volumes of distribution that could be quantified using both 1- or 2-tissue compartment models.<sup>4,7–9</sup>

The [11C]UCB-J tracer has already been investigated in human disease. A unilateral reduction of [11C]UCB-J binding was found at the seizure onset zone in the hippocampus of 3 patients with temporal lobe epilepsy.<sup>8</sup> In 10 Alzheimer's disease patients, a significant reduction in hippocampal [11C]UCB-J binding was seen compared to 11 cognitively healthy controls.<sup>11</sup> In schizophrenia patients, [11C]UCB-J binding was found to be decreased in the frontal and anterior cingulate cortex compared to healthy controls.<sup>12</sup> A pilot study of 2 Parkinson's disease patients found reduced [11C]UCB-J binding in the substantia nigra<sup>13</sup> and a study of 12 Parkinson's disease patients showed decreased [11C]UCB-J binding in the substantia nigra, red nucleus and locus coeruleus compared to 12 matched controls.<sup>14</sup> Furthermore, the severity of depressive symptoms was inversely correlated with [11C]UCB-J binding in 26 unmedicated patients with major depressive disorder or post-traumatic stress disorder. In individuals with severe depression, reduced [11C]UCB-J binding targeted the dorsolateral prefrontal cortex, anterior cingulate cortex and hippocampus.<sup>15</sup>

Rodents are routinely used as models of neurodegenerative and inflammatory disease, to study mechanisms of drug addiction, basic brain functions, and to test target occupancy, efficacy and toxicity of new drugs. Since [11C]UCB-J was used in clinical PET studies of human disease prior to its complete characterization in rodents, we were motivated to trial the radioligand in intact rodents and to explore the possibilities of studying altered synaptic density in animal lesion models of disease. For this study, the rat was chosen as its brain is larger than that of the mouse, improving the definition and resolution of PET signals from different brain areas.

Here we perform PET imaging on naïve rats in order to investigate the kinetics, metabolism and regional distribution of [11C]UCB-J. We also examine the *in vivo* specificity of the tracer binding by injecting different doses of the SV2A ligand levetiracetam (LEV) prior to [11C]UCB-J injection followed by PET imaging. We compare 1- and 2-tissue compartment models for describing brain [11C]UCB-J uptake kinetics and investigate whether a blood population input function can be used in the future. Further, we study UCB-J binding in a unilateral rat model of acute Parkinson's disease, induced by striatal injections of 6-hydroxydopamine (6-OHDA) and a unilateral rat model of acute Huntington's disease, induced by striatal injections of quinolinic acid (QA). We test the hypothesis that decreases in UCB-J binding will occur in the ipsilateral striatum in response to synaptic loss in both these disease models.

## Methods

### Rats and disease models

All experiments were approved by the Danish Animal Experiments Inspectorate (AEI) and performed in compliance with Danish laws and regulations for the Humane Care and Use of Animals in Research. Experiments were reported according to the ARRIVE guidelines. Female Sprague-Dawley rats (Taconic Biosciences, Inc.) were housed two to three per cage and maintained in a daily 12-h light cycle with *ad libitum* access to water and food. Nine naïve rats were used for basic investigations of brain [11C]UCB-J uptake kinetics with PET. To produce a hemi Parkinson model, rats received right intra-striatal injections of 6-hydroxydopamine (6-OHDA) (Janvier) ( $n=3$ ). A unilateral Huntington's disease model was prepared by injecting different doses of quinolinic acid (QA) into the right striatum (Taconic) ( $n=12$ ). Behavioral testing was performed post lesioning with the cylinder test along with microPET imaging. The rats weighed 250 at the time of surgery and approximately 270 g at the time of microPET imaging.

### [11C]UCB-J microPET imaging

The [11C]UCB-J tracer was produced using a modification of the method reported by Nabulsi et al.<sup>4</sup> For pilot studies, precursor was provided by UCB Pharma (Belgium). Additional precursor was purchased from Trasis (Belgium) and Pharmasynth (Estonia). Rats were anaesthetized using isoflurane (2.5%, Zoetis). A catheter was placed in the femoral artery for blood sampling and in the tail vein for tracer injection (radiochemical purity =  $99.2 \pm 1.0\%$ ,

specific activity =  $137.8 \pm 86$  GBq/ $\mu\text{mol}$ , injected activity =  $31.4 \pm 7.8$  MBq and injected mass =  $0.14 \pm 0.10$   $\mu\text{g}$ ). There were no differences in injected activity, volume, mass or specific activity between rats scanned at baseline and those scanned after blocking with LEV. Rats were placed prone in a plastic stereotaxic frame designed to fit in the gantry of the microPET (nanoscan microPET/1 T MRI, Mediso Ltd., Budapest, Hungary) and imaged for 90 min. During imaging, body temperature was kept at 36–36.5°C using integrated hot-air channels in the chamber wall.

### Blood curves

Arterial blood sampling ( $\sim 150$   $\mu\text{L}$  per sample) was conducted continuously during the first 90 s post iv injection and then again after 5, 10, 20, 30, 45, 60, 75 and 88 min. No blood was sampled from the rats injected with 6-OHDA. Radioactivity in 50  $\mu\text{L}$  whole blood and 50  $\mu\text{L}$  plasma samples (prepared by centrifugation at 4°C, 21,000 $\times g$ , 2 min) were counted in a gamma-counter (Cobra II, Packard Instrument Co.) and cross-calibrated to the microPET scanner.

### Metabolism

Blood samples ( $\sim 200$   $\mu\text{L}$  per sample) for metabolite correction were collected after 5, 10, 20, 40, 60 and 80 min. Acetonitrile (1:1) was added to 100  $\mu\text{L}$  plasma and centrifuged (4°C, 21,000 $\times g$ , 5 min). The un-metabolized parent fraction was determined in the plasma samples using radio-HPLC with a Luna C18 (2) semi-preparative column (10  $\times$  250 mm, 5  $\mu\text{m}$ , Phenomenex) and a mobile phase consisting of 50% acetonitrile in 70 mM  $\text{NaH}_2\text{PO}_4$  (v/v, pH 4.5) at a flow rate of 5 ml/min. The HPLC fractions were collected with an automated fraction collector (0.5 min/well) and radioactivity was counted on an automated gamma-counter.

### PET data reconstruction

PET data were reconstructed and binned as 26 time-frames (8  $\times$  15, 4  $\times$  30, 2  $\times$  60, 2  $\times$  120, 4  $\times$  300 and 6  $\times$  600 s), 0.7 mm voxel resolution, 2 mm FWHM resolution, 3D Tera-Tomo and maximum likelihood expectation maximization (MLEM) reconstruction. PMOD 3.6 software (PMOD Technologies Ltd, Zurich, Switzerland) was used to co-register the PET images to a rat T2-weighted MR template using rigid transformation. Volumes of interest (VOIs)<sup>16</sup> defined on this PMOD rat brain template were used to generate time activity curves for further analyses.

### Data analysis

Brain time activity curves (TACs) were generated by sampling brain VOIs to examine the uptake and wash-out kinetics of the tracer. The brain kinetics of the TACs were then interrogated for goodness of fit using 1- and 2-tissue compartment models (1T and 2T) in order to calculate volume of distribution ( $V_T$ ). Goodness of each fit was determined by the Akaike Information Criterion (AIC) and the standard error (SE). To determine the occupancy by LEV at different doses, a Lassen occupancy plot was applied across all the defined VOIs. The plasma-free fraction ( $f_p$ ) was determined as described earlier<sup>17</sup> using plasma from four rats. We also calculated  $k_3/k_4$  as an estimate of binding potential; however, due to the high standard error associated with this estimation and the large variability (up to 100%) across animals, we do not present these data.

### Population-based plasma input function

Population-based TACs for [11C]UCB-J and its metabolites were generated for whole blood and plasma based on nine naïve rats. The population-based metabolite curve was generated by directly averaging the individual metabolite curves. Population-based whole blood and plasma curves were made by correcting individual curves for injected dose and weight. All individual curves were interpolated and the peaks were aligned to the average peak before averaging them to produce a standard input function. This standard input function could then be back corrected for injected dose and weight in order to use it for modelling brain TACs of individual rats.

### Occupancy

LEV was used to block [11C]UCB-J binding and estimate the non-displaceable distribution volume ( $V_{ND}$ ) and tracer occupancy. Four of the naïve rats were PET scanned again after their initial baseline scan. The second blocked scan was similar to the baseline scan except for the prior administration of different doses of LEV (10 mg/kg ( $n=1$ ), 40 mg/kg ( $n=1$ ) and 100 mg/kg ( $n=2$ )) in the tail vein 1–2 min before start of [11C]UCB-J PET.

### Intrastriatal injections

The 6-OHDA solution (20  $\mu\text{g}/4$   $\mu\text{L}$ ) was prepared using a 0.02% ascorbic acid solution diluted in sterile water. To get a 5  $\mu\text{g}/\mu\text{L}$  100% free base 6-OHDA solution, 6.1 mg/mL 82% free base 6-OHDA powder (Sigma-Aldrich) was added to the ascorbic acid solution just before the surgery started. This was usable for 2 h when

stored on ice and protected against light. The quinolinic acid solution (20 µg/4 µL or 40 µg/8 µL) was prepared according to Lelos et al.<sup>18</sup>

Rats were anaesthetized (1.8 mL per rat i.p. of a mixture of 0.8 mL Cepetor and 10 mL Fentanyl-Hameln), and placed in a stereotaxic frame after shaving their scalp. A cut was made and a small hole was drilled in the scalp for the intrastriatal injections. The Hamilton syringe cannula tips were sited at the appropriate coordinates (6-OHDA; AP: 1, MC: -3 and DV: -4.9; QA (20 µg) AP: 1, MC: -3 and DV: -4.8; QA (40 µg (2 × 20 µg)) injection site 1; AP: -0.4, MC: -4 and DV: -4/-5 (two deposits of 2 µL at different depths), site 2; AP: 1.2, MC: -3.2 and DV: -3.5/-4.5). The volume was injected at a rate of 0.3 µL every 30 s. After the injection, the cannula was left in place for 5 min before removal. The opening was closed with suture wound clips. Temgesic (0.3 mL) and antisedan (0.35 mL, diluted using 2 mL antisedan in 18 mL saline) were given subcutaneously to relieve pain and wake up the rat, respectively.

### Cylinder test

Each rat was placed in a Plexiglas cylinder for 5 min while its movements were recorded on video. The number of forelimb touches on the cylinder wall was recorded, which enabled analysis of spontaneous use of the forelimbs<sup>19,20</sup> by an investigator blinded to the groups.

### Autoradiography

After the PET scan, rats were euthanized using i.p. injections of pentobarbital followed by removal and fresh freezing of the brain. The brains were cut into 20 µm thick coronal slices, mounted on poly-L-lysine-coated slides (4 slices per slide, Thermo Scientific) and stored at -80°C.

The slides were left to thaw at room temperature and pre-washed for 5 min in 50 mM Tris-HCl buffer (pH=7.4). For each rat, two slides were used to assess total binding and one for non-specific binding. The total binding-slides were incubated with 3 nM [3H]UCB-J (specific activity 82 Ci/mmol, Cat. No.: NT1099, Novandi Chemistry AB, Sweden) in buffer, while slides for non-specific binding were incubated in the same concentration of radioligand, but in the presence of LEV (900 µM) for 60 min. All slides were post-washed for 2 × 1 min in buffer, dipped briefly in Milli-Q water (4°C), dried under a stream of cold air and read for 2 h using BeaQuant v. 1.14 (ai4r, France) prior to analysis using Beamage v.2.1.7 software. Background binding was subtracted and specific binding was obtained by subtracting the non-specific binding from

the total binding. Values were calibrated to an in-house standard with known radioactive concentration. Due to technical problems where the tissue did not stick properly to the slides around the injection site when performing autoradiography in tissue obtained from the 6-OHDA rat model, we only present data in moderate and high dose QA-injected rats.

### Statistics

Akaike information criteria (AIC) and standard errors (SE) of  $V_T$  were used to compare  $V_T$  values generated by the 1T and 2T models. When blocking with LEV, the gradient of the linear Lassen occupancy plot represented its percentage occupancy. For the population input function, the percentage error of estimation of the AUC (%error AUC)<sup>21</sup> and the  $V_T$  (% error  $V_T$ ) were calculated for original input functions and for the population-based input function (PBIF) for each rat for comparison. For the 6-OHDA and QA experiments, paired *t*-tests were used to interrogate side-to-side differences in the cylinder test, [3H]UCB-J autoradiography and [11C]UCB-J PET.

## Results

### PET image analysis in naïve rats

[11C]UCB-J was metabolized rapidly with a baseline parent fraction of 65, 46, 31, 24, 20 and 20% after 5, 10, 20, 40, 60 and 80 min and a retention time of ~7 min. Representative [11C]UCB-J binding images and [11C]UCB-J uptake values are shown in Figure 1. A high and rapid uptake was observed after iv injection with peak uptake times of 17.5–35 min in the striatum and 22.5–35 min in the frontal cortex under baseline conditions. The plasma free fraction was  $0.278 \pm 0.016$ .

Injection of different blocking doses of LEV prior to PET imaging, resulted in reduced uptake of [11C]UCB-J (see Figure 1), an earlier peak and a faster clearance, confirming its specific SV2A binding.

### Kinetic modeling

Comparing the utility of the 1T and 2T models, the 2T model generated lower  $V_T$  standard errors and AIC values (see Table 1), but one of the nine baseline scans could not be accurately modeled. The mean difference between  $V_T$  values generated by the 1T or 2T model (in eight baseline scans) was 3.5%. Thus, the 1T model proved more robust and, since the  $V_T$  values generated from the 1T and 2T models were very similar, the 1T model was used for further analyses.

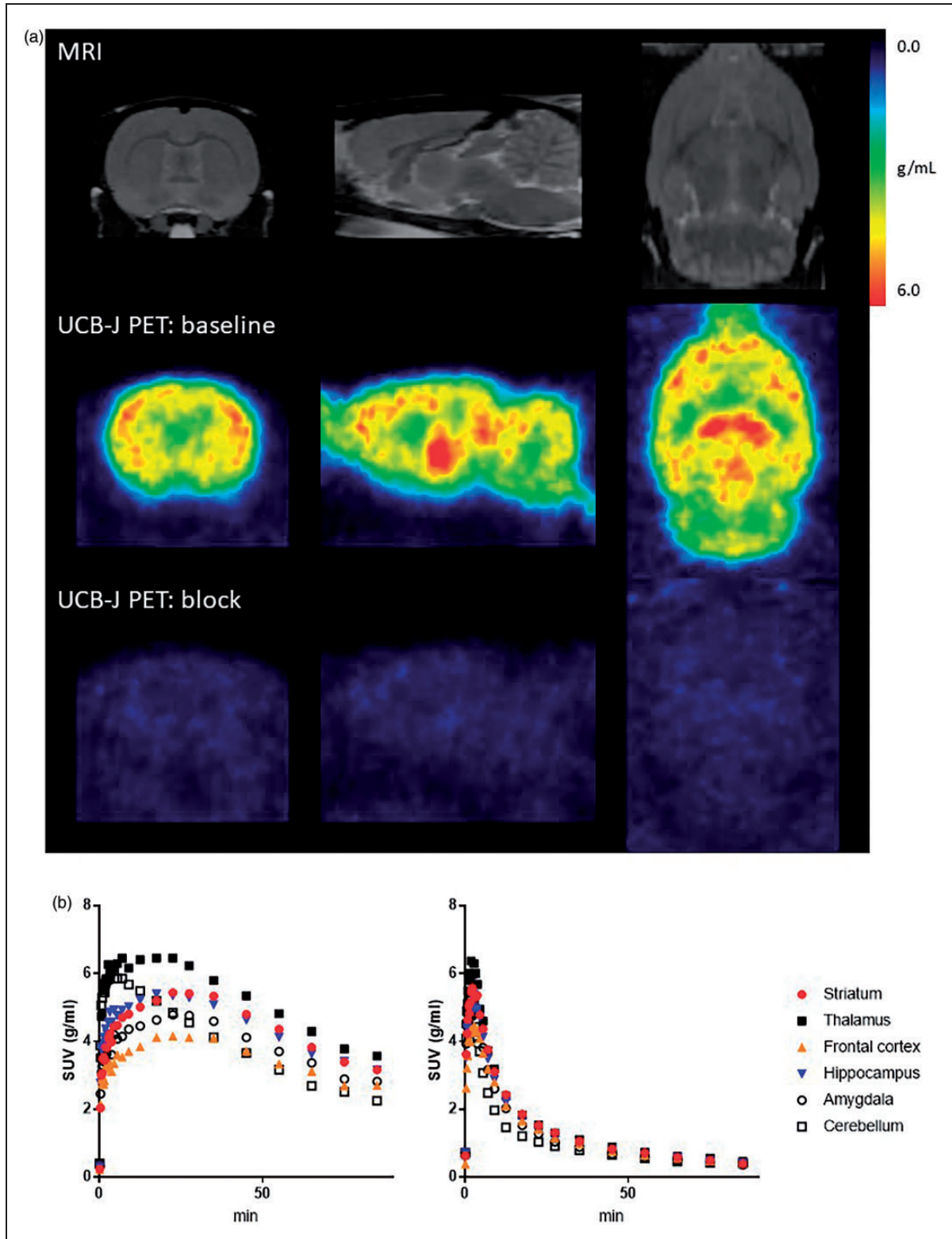


**Figure 1.** [ $^{11}\text{C}$ ]UCB-J PET in naive rodent brain. (a) Rat MRI template (top) and representative standard uptake value (SUV) images (average of 30–90 min) of [ $^{11}\text{C}$ ]UCB-J PET scan at baseline condition (middle) and after administration of 100 mg/kg LEV (bottom) in the same rat shown at the coronal (left), sagittal (middle) and transverse (right) plane. (b) Representative SUV time activity curves at baseline condition (left) and after administration of 100 mg/kg LEV (right) in the same rat.

**Table 1.** [11C]UCB-J PET imaging kinetics of the 1- and 2-tissue compartment models in naïve rats.

Brain region		$V_T$ (ml/cm <sup>3</sup> )	SE of $V_T$	AIC	KI (ml/cm <sup>3</sup> /min)	$V_T(2T) = a * V_T(1T) + b$
Striatum	1T	44.6 (10.3)	4.9 (3.1)	40.7 (30.9)	1.7 (1.3)	a = 1.23
	2T	46.6 (13.0)	4.5 (4.1)	30.4 (30.9)	3.4 (3.0)	b = -8.32
Frontal cortex	1T	41.8 (8.1)	4.9 (1.1)	39.4 (18.3)	1.2 (0.9)	a = 1.72
	2T	43.3 (8.8)	4.9 (1.8)	31.1 (17.2)	2.4 (2.6)	b = -5.57
Hippocampus	1T	41.8 (9.6)	5.2 (0.5)	46.7 (14.0)	1.3 (0.9)	a = 1.22
	2T	43.9 (10.1)	5.3 (1.2)	36.7 (11.8)	2.8 (2.6)	b = -6.85
Thalamus	1T	46.2 (10.8)	5.0 (0.9)	42.7 (18.7)	1.6 (1.2)	a = 1.19
	2T	48.2 (10.9)	4.9 (1.0)	32.3 (17.3)	3.1 (2.6)	b = -6.69
Amygdala	1T	38.0 (9.1)	5.3 (0.5)	46.7 (13.0)	1.1 (0.8)	a = 1.22
	2T	39.9 (9.6)	4.9 (0.8)	37.1 (11.2)	2.8 (2.6)	b = -6.44
Cerebellum	1T	31.6 (8.2)	5.5 (1.2)	50.6 (17.2)	1.5 (1.2)	a = 1.14
	2T	33.5 (8.1)	5.1 (1.3)	36.1 (21.9)	3.1 (2.7)	b = -2.42

Note: Mean values of volume of distribution ( $V_T$ ), standard error (SE) of  $V_T$ , Akaike information criterion (AIC), KI and linear regression values from correlations between  $V_T$  estimated using the 1- or 2TCM (see the corresponding graphs in Supplemental Figure 1). N = 8.

### UCB-J blockade

LEV was used to block [11C]UCB-J binding.  $V_{ND}$  and occupancies were estimated with the occupancy plot (Figure 2) using 10 mg/kg ( $n=1$ ), 40 mg/kg ( $n=1$ ) and 100 mg/kg ( $n=2$ ) doses of LEV. These resulted in 33%, 78% and 82% occupancy showing specific binding.  $V_{ND}$  estimated from the 100 mg/kg LEV was 2.51.

### Population-based input function

We attempted to generate PBIFs from our blood samples but these yielded AUC% errors of  $15.16 \pm 5.3$  and  $15.09 \pm 10.78$  for whole blood and plasma, respectively, and  $V_T$ % errors of  $18.76 \pm 18.64$ . Even though these errors were considered high, we tested PBIFs in our rat models of disease.

### Cylinder test in rat models of disease

To evaluate the sensitivity of [11C]UCB-J PET for detecting synaptic SV2A loss in rat models of disease, we performed PET imaging in rat models of Parkinsonism, induced unilaterally with a right striatal injection of 6-OHDA, and of Huntington's disease, induced unilaterally with a right striatal injection of QA. Since both models involve basal ganglia, the cylinder test was used to assess motor defects.

*Forelimb akinesia* was evaluated in rats unilaterally injected with 6-OHDA seven weeks post-surgery and those receiving QA approximately four weeks after surgery. A tendency for the 6-OHDA rats to use the right forelimb was observed ( $p$ -value = 0.068). No paw preference was observed in the 20  $\mu$ g QA-injected rats, while a clear preference for use of the right forelimb was seen in the 40  $\mu$ g QA rats (Figure 3), indicating

unilateral loss of motor activity connected to the striatum.

*[11C]UCB-J PET analysis in rat models of disease.* [11C]UCB-J PET showed a unilateral loss of striatal synaptic SV2A density ipsilateral to the injection site in both the 6-OHDA and QA rat models. When comparing the decrease in the SUV values acquired during three time windows (30–90 min, 60–90 min and 40–60 min) to matched  $V_T$  values in the QA lesioned rats, the 60–90 min SUV interval data showed the best correlation (30–90 min SUV:  $r^2=0.65$ ,  $p$ -value = 0.0088, 60–90 min SUV:  $r^2=0.66$ ,  $p$ -value = 0.0075, 40–60 min SUV:  $r^2=0.64$ ,  $p$ -value = 0.0099). As no blood was sampled from the 6-OHDA lesioned rats, the 60–90 min SUV interval was used to determine the striatal UCB-J decrease. Only a small  $6.2 \pm 2.52\%$  SUV but significant decrease was seen in the right striatal injection area compared to the corresponding left side of the 6-OHDA rats (Figures 4 and 5, Table 2). A  $39.3 \pm 7.98\%$  and  $55.1 \pm 5.59\%$   $V_T$  ( $31.0 \pm 8.16\%$  and  $49.6 \pm 6.72\%$  SUV) significant decrease was seen in the right striatal injection area compared to the corresponding left in the 20  $\mu$ g and 40  $\mu$ g QA rat model, respectively (Figures 4 and 5, Table 2).

### Autoradiography

[3H]UCB-J autoradiography analysis of the QA rat model confirmed unilateral  $38.4 \pm 8.03\%$  ( $p$ -value < 0.0001) and  $52.5 \pm 3.69\%$  ( $p$ -value = 0.0052) loss of synaptic SV2A binding ipsilateral to the right injection side in the 20  $\mu$ g QA and 40  $\mu$ g QA model, respectively (see Figure 6 and Table 2). The in vivo PET versus autoradiography asymmetries of all QA-injected rats are shown in Supplemental Figure 2.

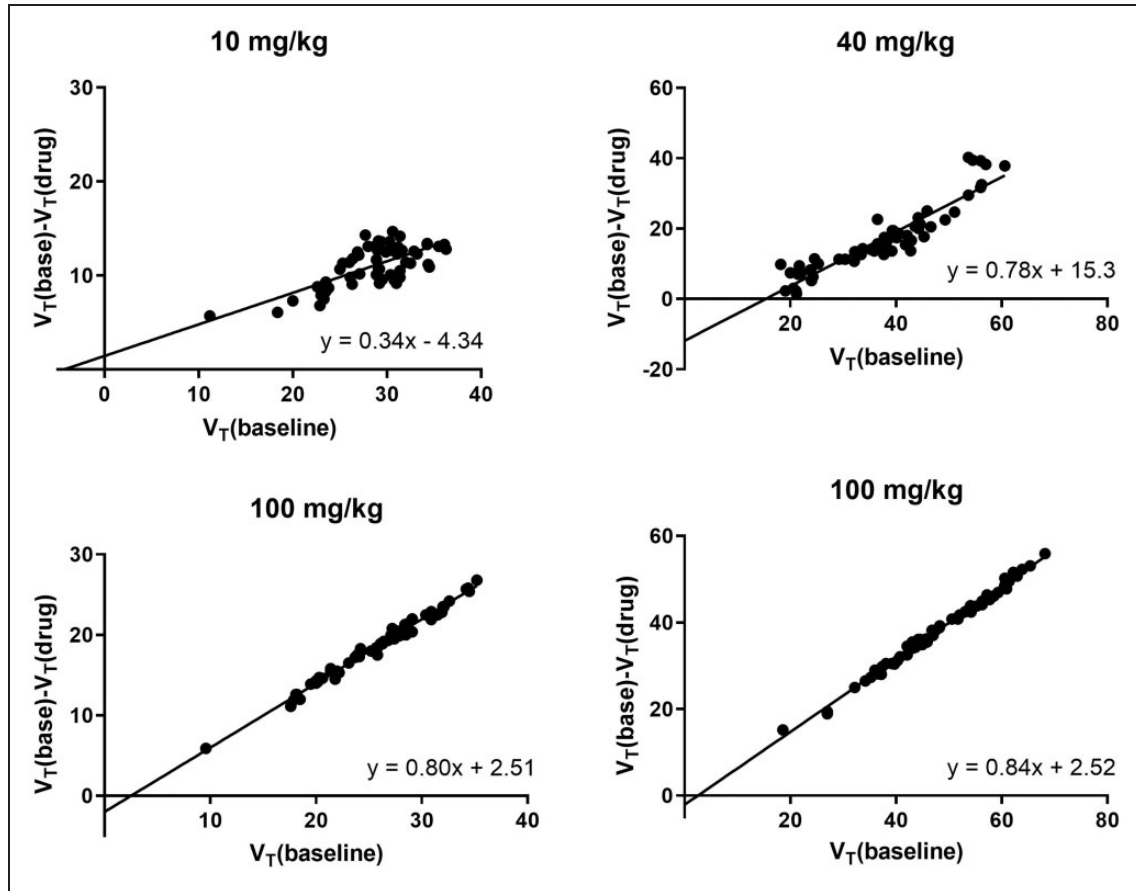


**Figure 2.** Occupancy plot for four blocking scans using different doses of levetiracetam (LEV). At a dose of 10 mg/kg,  $V_{ND} = -4.33$  and occupancy = 33%. At a dose of 40 mg/kg,  $V_{ND} = 15.33$  and occupancy = 78%. At a dose of 100 mg/kg,  $V_{ND} = 2.51$  and occupancy = 80–84%.

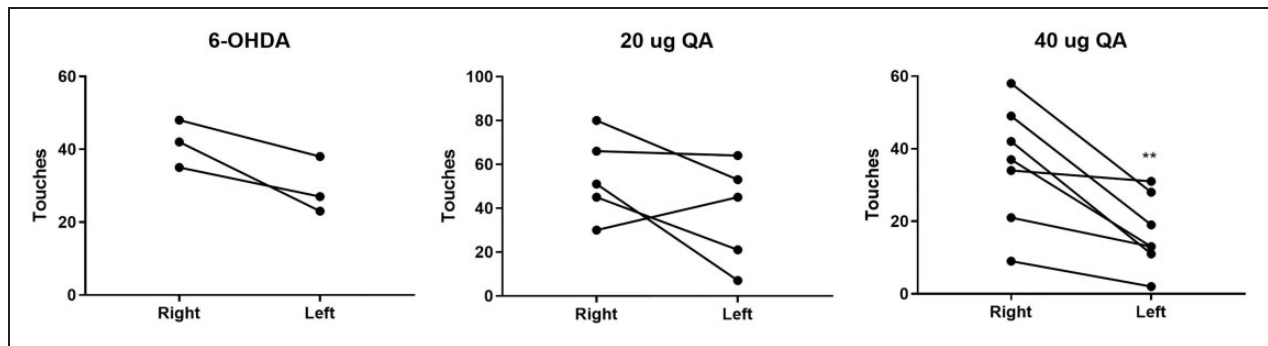


**Figure 3.** Rodent model validation using the cylinder test. Number of left and right forelimb touches on the cylinder wall during 3 min of testing in rats injected into the striatum with 6-hydroxydopamine (6-OHDA) (left), 20 µg Quinolinic acid (QA) (middle) or 40 µg QA (right). \*\*p-value < 0.01

**Discussion**

In this paper, we have evaluated the in vivo [11C]UCB-J PET signal in naïve rats and performed studies in toxin-induced rat models of acute Parkinson’s and

Huntington’s disease using in vivo microPET and post-mortem autoradiography methods.

The non-metabolized parent fraction found here was similar to that previously reported<sup>4</sup> confirming fast

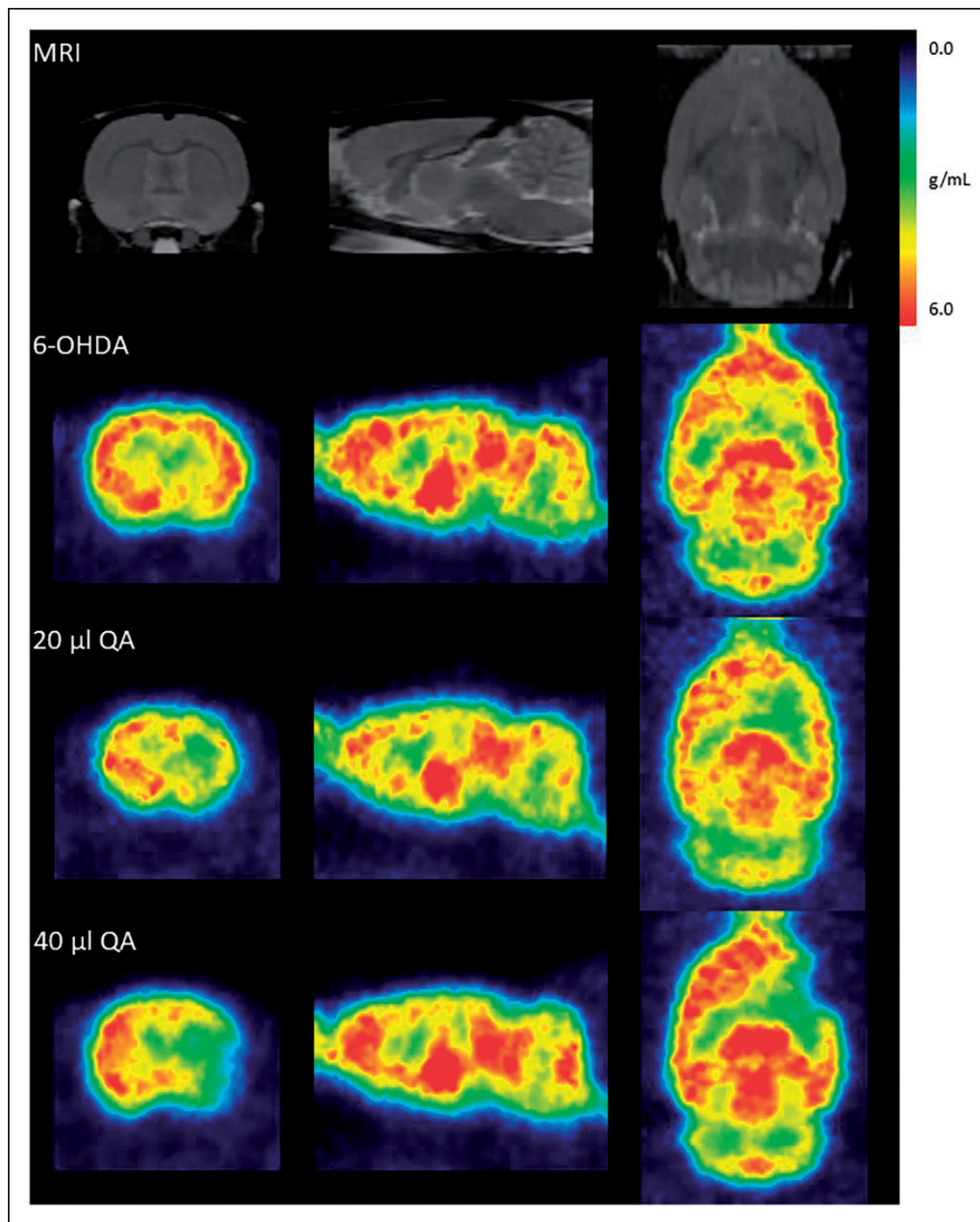


**Figure 4.** [ $^{11}\text{C}$ ]UCB-J PET in unilateral models of neurodegeneration. Rat MRI template (top) and representative SUV images of [ $^{11}\text{C}$ ]UCB-J PET after injection of 6-hydroxydopamine (6-OHDA), 20  $\mu\text{g}$  Quinolinic acid (QA) or 40  $\mu\text{g}$  QA into the right striatum, shown at the coronal (left), sagittal (middle) and transverse (right) plane.

systemic tracer metabolism in rats. In the intact rat, we see highest [ $^{11}\text{C}$ ]UCB-J binding to synaptic SV2A in the thalamus and striatum, moderate binding in the frontal cortex, hippocampus and amygdala and low binding in the cerebellum. This is similar to reported [ $^{11}\text{C}$ ]UCB-J binding in humans, where high binding

was seen in the striatum, frontal cortex and amygdala and lower binding in the hippocampus, thalamus and cerebellum.<sup>7</sup>

The  $V_T$  values computed were similar when using 1T and 2T models to describe the kinetics of brain TACs, thus suggesting that both models can be used in further studies.



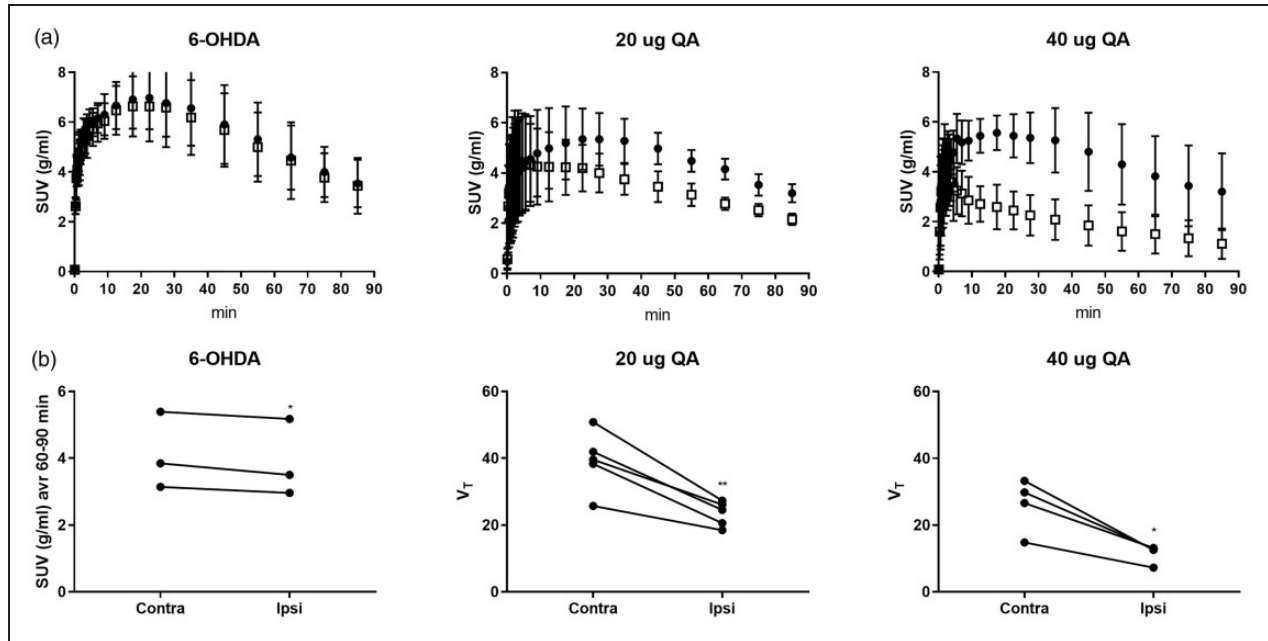


**Figure 5.** (a) Striatal standard uptake value (SUV) time activity curves in 6-hydroxydopamine (6-OHDA, left), 20 µg Quinolinic acid (QA, middle) and 40 µg QA (right) rats. (b) [ $^{11}\text{C}$ ]UCB-J PET SUV values (average of 60–90 min) or  $V_T$  in the left and right striatal injection area after injection of 6-OHDA (left), 20 µg QA (middle) and 40 µg QA (right) into the right striatum. \* $p$ -value < 0.05, \*\* $p$ -value < 0.01.

**Table 2.** Unilateral striatal loss (% of contralateral) detected by [ $^{11}\text{C}$ ]UCB-J PET imaging and [ $^3\text{H}$ ]UCB-J autoradiography in animal models of disease.

	6-OHDA	20 µg QA	40 µg QA
[ $^{11}\text{C}$ ]UCB-J PET imaging, SUV	6.2 (2.52)	31.0 (8.16)	49.6 (6.72)
[ $^{11}\text{C}$ ]UCB-J PET imaging, $V_T$		39.3 (7.98)	55.1 (5.59)
[ $^{11}\text{C}$ ]UCB-J PET imaging, $V_T$ , PBIF	8.46 (2.30)	37.8 (8.00)	54.6 (7.02)
[ $^3\text{H}$ ]UCB-J autoradiography		38.4 (8.03)	52.5 (3.69)

Note: Mean unilateral striatal loss (% of contralateral) detected by [ $^{11}\text{C}$ ]UCB-J PET imaging and [ $^3\text{H}$ ]UCB-J autoradiography in animal models of disease (6-hydroxydopamine (6-OHDA), quinolinic acid (QA)). Values are presented as mean (SD).

Here we chose to use the 1T model as PET imaging data from all nine rats could be fitted using this model, while the fit of one rat was unacceptable with the 2T model. The high K1 observed in the current rat study, and in the previous work in mouse,<sup>9</sup> suggests an extensive first pass extraction into the rodent brain. Brain uptake may, therefore, be flow limited due to rapid trapping in a bound compartment. As tracer uptake took 20 min to peak after injection and varied across grey matter regions known to have similar levels of blood flow, it seems unlikely that flow determined its uptake. In human studies, K1 values have been reported to be in a more physiological range.<sup>11</sup>

UCB-J was initially developed alongside two other SV2A ligands, UCB-A and UCB-H.<sup>22</sup> PET uptake of [ $^{18}\text{F}$ ]UCB-H has previously been investigated in rats.<sup>23</sup> As in the current study, they found high and rapid brain uptake with highest binding of the tracer in the thalamus and striatum, moderate binding in

hippocampus and cortex and low binding in the cerebellum. UCB-J shows higher specific binding compared to UCB-H in rhesus monkeys,<sup>4</sup> which has resulted in greater focus on its use.

LEV is an antiepileptic drug that binds to vesicular SV2A protein. The antiepileptic mechanism of the drug is still uncertain, but it inhibits presynaptic calcium channels,<sup>24</sup> which are essential to neurotransmitter release. Here, injection of 10, 40 and 100 mg/kg LEV before scan start resulted in 33%, 78% and 82% dose-dependent drug occupancy of the SV2A binding site and confirming specific binding of [ $^{11}\text{C}$ ]UCB-J.

Even though  $V_T$  values derived from a simple PBIF in this study showed high variability, the unilateral loss of binding seen in the QA lesioned rats was similar whether using  $V_{T,PBIF}$  or  $V_T$ . It is possible that a more accurate PBIF could be generated and used in the future if a more accurate blood sampling method

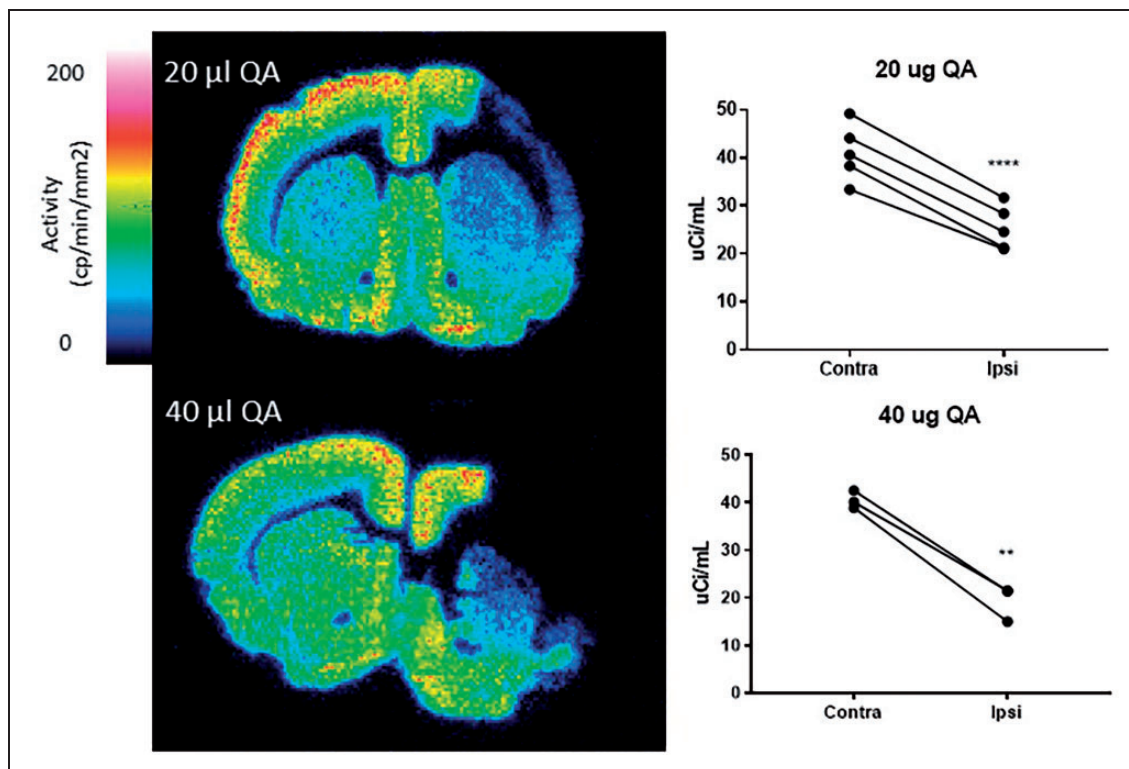


**Figure 6.** [3H]UCB-J autoradiography images of representative animals after unilateral lesion to the right striatum with 20 µg QA (top) and 40 µg QA (bottom). Graphs to the right of each image show [3H]UCB-J autoradiography values in the contra- and ipsilateral striatum in each model. \*\**p*-value < 0.01, \*\*\*\**p*-value < 0.0001.

was available. For example, a  $\beta$ -microprobe system could be used to measure blood activity continuously (every 1 s). Mice have a small blood volume which makes blood sampling problematic. In one [11C]UCB-J study, an input function was generated by imaging total blood radioactivity of the heart sampling activity with a volume of interest over the left ventricle.<sup>9</sup> In contrast to rat PET imaging studies, the small size of the mouse allows a larger PET field of view and activity of both brain and the heart can be imaged simultaneously. In another mouse study, blood sampling was avoided by normalizing SUV values to whole brain or brainstem SUV values. This approach detected decreased hippocampal binding in a transgenic mouse model of Alzheimer's disease compared to wild-type mice.<sup>10</sup>

Ipsilateral striatal synaptic loss was seen in our rat models of unilateral disease whether they were injected with 6-OHDA or QA. This was accompanied by impaired contralateral limb motor function when performing the cylinder test. Striatal 6-OHDA injections can induce limb bradykinesia in the rat similar to that seen in Parkinson's disease as they target dopaminergic (and noradrenergic) neurons and induce nigral cell death by a dying back mechanism. It has been

suggested that the neurotoxicity of 6-OHDA arises from inhibition of the mitochondrial respiratory chain resulting in oxidative stress and reactive oxygen species.<sup>25</sup> Previous PET imaging studies with 6-OHDA rats have shown reduced striatal uptake of the dopamine precursor [18F]-6-fluorodopa (FDOPA) and also of the vesicular monoamine transporter (VMAT2) ligand [11C]dihydrotrabenazine (DTBZ).<sup>26</sup> We found a 6.2% decrease in striatal [11C]UCB-J binding in our group of 6-OHDA rats. This small decrease is in line with current views that nigral dopaminergic projections constitute only around 10% of striatal terminals<sup>27,28</sup> so a 6.2% loss of SV2A binding is predictable and physiologically significant.

QA is a metabolite of the kynurenine pathway and acts as an agonist at NMDA ion channel complexes. QA exerts neurotoxicity by increasing Ca flux into neurons via the NMDA ion channels, disturbing the cytoskeleton, generating free radicals and oxidative stress and by causing lipid peroxidation.<sup>29</sup> Chronic exposure can cause structural changes affecting the microtubular distribution and a decrease in organelles. Structures such as the striatum and hippocampus, where NMDA ion channels are dense, are especially susceptible to QA toxicity. Neurons particularly sensitive to QA include

striatal cholinergic interneurons, hippocampal pyramidal neurons and striatal GABAergic spiny projection neurons of the direct pathway containing substance P. Striatal spiny neurons containing somatostatin and neuropeptide Y are unaffected.<sup>29</sup> This sparing of somatostatin and neuropeptide Y positive medium spiny neurons in the striatum alongside striking GABA spiny neuronal cell death resembles the pathology of Huntington's disease.<sup>30</sup> In our experiment, we saw a significant effect of QA toxicity on striatal SV2A binding. The adjacent cortex was affected to a small extent when using 20 µg QA but to a larger extent when using 40 µg QA. Thus, the effect we see here, with 6.2%, 39.3% and 55.1% decreases in striatal SV2A binding in rats lesioned with 6-OHDA, 20 µg QA and 40 µg QA, respectively, reflects both toxin doses and the different densities of dopaminergic and GABAergic interneuron terminals in the striatum. In the QA-lesioned rats, we were able to show similar decreases in SV2A binding using autoradiography in fresh frozen brain slices. As a final note, if we assume a  $K_d$  in rat of 6.8 nM, we estimate a self-occupancy of 31% when administering a dose of 3 nM [3H]UCB-J. As we are not concerned about physiological/pharmacological effects in autoradiography studies, we do not expect a partial blockade to significantly change our interpretation of the data aside from a potential underestimation of binding.

In conclusion, we have shown that [11C]UCB-J PET is a good in vivo marker of synaptic SV2A density in the rat brain. This opens the possibility to non-invasively investigate in vivo synaptic density longitudinally and in response to therapy in animal models of neurodegenerative diseases.

### Funding

The author(s) disclosed receipt of the following financial support for the research, authorship, and/or publication of this article: The project was supported by the Lundbeck Foundation, Parkinsonforeningen, Fonden af 2/7 1984 til Bekæmpelse af Parkinsonsyge and Aarhus University.

### Acknowledgements

We thank UCB Pharma for providing tracer precursor for pilot studies. We are grateful to the staff at the Aarhus University Hospital PET Centre and Aarhus University for assistance.



### Declaration of conflicting interests

The author(s) declared no potential conflicts of interest with respect to the research, authorship, and/or publication of this article.

### Authors' contributions

MBT, MRR, DJB and AML designed the studies. JJ and ACS synthesized the radioligand and MS imaged the rats. MBT and MRR prepared the 6-OHDA and QA rodent models and performed behavioural studies. MBT performed the autoradiography and MBT and TPL analysed and interpreted the micropet and autoradiography data under the supervision of AML. MBT wrote the first draft of the manuscript with support from AML. All authors have provided suggestions and edits, and have approved the final version of the manuscript.

### ORCID iDs

Thea P Lillethorup  <https://orcid.org/0000-0003-1692-5975>  
Anne M Landau  <https://orcid.org/0000-0002-7371-8713>

### Supplemental material

Supplemental material for this article is available online.

### References

- Picconi B, Piccoli G and Calabresi P. Synaptic dysfunction in Parkinson's disease. *Adv Exp Med Biol* 2012; 970: 553–572.
- Jang BG, In S, Choi B, et al. Beta-amyloid oligomers induce early loss of presynaptic proteins in primary neurons by caspase-dependent and proteasome-dependent mechanisms. *Neuroreport* 2014; 25: 1281–1288.
- Rozas JL, Gomez-Sanchez L, Tomas-Zapico C, et al. Presynaptic dysfunction in Huntington's disease. *Biochem Soc Transac* 2010; 38: 488–492.
- Nabulsi NB, Mercier J, Holden D, et al. Synthesis and preclinical evaluation of 11C-UCB-J as a PET tracer for imaging the synaptic vesicle glycoprotein 2A in the brain. *J Nucl Med* 2016; 57: 777–784.
- Bajjalieh SM, Frantz GD, Weimann JM, et al. Differential expression of synaptic vesicle protein 2 (SV2) isoforms. *J Neurosci* 1994; 14: 5223–5235.
- Calhoun ME, Jucker M, Martin LJ, et al. Comparative evaluation of synaptophysin-based methods for quantification of synapses. *J Neurocytol* 1996; 25: 821–828.
- Finnema SJ, Nabulsi NB, Mercier J, et al. Kinetic evaluation and test-retest reproducibility of [(11)C]UCB-J, a novel radioligand for positron emission tomography imaging of synaptic vesicle glycoprotein 2A in humans. *J Cereb Blood Flow Metab* 2017; 38: 2041–2052.
- Finnema SJ, Nabulsi NB, Eid T, et al. Imaging synaptic density in the living human brain. *Sci Transl Med* 2016; 8: 348ra96.
- Bertoglio D, Verhaeghe J, Miranda A, et al. Validation and noninvasive kinetic modeling of [(11)C]UCB-J PET imaging in mice. *J Cereb Blood Flow Metab* 2019; 40: 1351–1362.
- Toyonaga T, Smith LM, Finnema SJ, et al. In vivo synaptic density imaging with (11)C-UCB-J detects treatment effects of saracatinib (AZD0530) in a mouse model of Alzheimer's disease. *J Nucl Med* 2019; 60: 1780–1786.

11. Chen MK, Mecca AP, Naganawa M, et al. Assessing synaptic density in Alzheimer disease with synaptic vesicle glycoprotein 2A positron emission tomographic imaging. *JAMA Neurol* 2018; 75: 1215–1224.
12. Onwordi EC, Half EF, Whitehurst T, et al. Synaptic density marker SV2A is reduced in schizophrenia patients and unaffected by antipsychotics in rats. *Nat Commun* 2020; 11: 246.
13. Cai Z, Li S, Matuskey D, et al. PET imaging of synaptic density: a new tool for investigation of neuropsychiatric diseases. *Neurosci Lett* 2019; 691: 44–50.
14. Matuskey D, Tinaz S, Wilcox KC, et al. Synaptic changes in Parkinson disease assessed with in vivo imaging. *Ann Neurol* 2020; 87: 329–338.
15. Holmes SE, Scheinost D, Finnema SJ, et al. Lower synaptic density is associated with depression severity and network alterations. *Nat Commun* 2019; 10: 1529.
16. Schiffer WK, Mirrione MM, Biegon A, et al. Serial microPET measures of the metabolic reaction to a microdialysis probe implant. *J Neurosci Meth* 2006; 155: 272–284.
17. Thomsen MB, Lillethorup TP, Jakobsen S, et al. Neonatal domoic acid alters in vivo binding of [11C] yohimbine to alpha2-adrenoceptors in adult rat brain. *Psychopharmacology* 2016; 233: 3779–3785.
18. Lelos MJ and Dunnett SB. Generating excitotoxic lesion models of Huntington's disease. *Meth Mol Biol* 2018; 1780: 209–220.
19. Stoltz S, Humm JL and Schallert T. Cortical injury impairs contralateral forelimb immobility during swimming: a simple test for loss of inhibitory motor control. *Behav Brain Res* 1999; 106: 127–132.
20. Sanchez-Guajardo V, Annibaldi A, Jensen PH, et al. alpha-synuclein vaccination prevents the accumulation of Parkinson disease-like pathologic inclusions in striatum in association with regulatory T cell recruitment in a rat model. *J Neuropathol Exp Neurol* 2013; 72: 624–645.
21. Shiozaki T, Sadato N, Senda M, et al. Noninvasive estimation of FDG input function for quantification of cerebral metabolic rate of glucose: optimization and multicenter evaluation. *J Nucl Med* 2000; 41: 1612–1618.
22. Mercier J, Archen L, Bollu V, et al. Discovery of heterocyclic nonacetamide synaptic vesicle protein 2A (SV2A) ligands with single-digit nanomolar potency: opening avenues towards the first SV2A positron emission tomography (PET) ligands. *Chem Med Chem* 2014; 9: 693–698.
23. Warnock GI, Aerts J, Bahri MA, et al. Evaluation of 18F-UCB-H as a novel PET tracer for synaptic vesicle protein 2A in the brain. *J Nucl Med* 2014; 55: 1336–1341.
24. Vogl C, Mochida S, Wolff C, et al. The synaptic vesicle glycoprotein 2A ligand levetiracetam inhibits presynaptic Ca<sup>2+</sup> channels through an intracellular pathway. *Mol Pharmacol* 2012; 82: 199–208.
25. Glinka Y, Gassen M and Youdim MB. Mechanism of 6-hydroxydopamine neurotoxicity. *J Neural Trans Suppl* 1997; 50: 55–66.
26. Walker MD, Dinelle K, Kornelsen R, et al. Measuring dopaminergic function in the 6-OHDA-lesioned rat: a comparison of PET and microdialysis. *EJNMMI Res* 2013; 3: 69.
27. Groves PM, Linder JC and Young SJ. 5-hydroxydopamine-labeled dopaminergic axons: three-dimensional reconstructions of axons, synapses and postsynaptic targets in rat neostriatum. *Neuroscience* 1994; 58: 593–604.
28. Uchigashima M, Ohtsuka T, Kobayashi K and Watanabe M. Dopamine synapse is a neuroligin-2-mediated contact between dopaminergic presynaptic and GABAergic postsynaptic structures. *Proc Natl Acad Sci U S A* 2016; 113: 4206–4211.
29. Lugo-Huitron R, Ugalde Muniz P, Pineda B, et al. Quinolinic acid: an endogenous neurotoxin with multiple targets. *Oxid Med Cell Longevity* 2013; 2013: 104024.
30. Beal MF, Kowall NW, Ellison DW, et al. Replication of the neurochemical characteristics of Huntington's disease by quinolinic acid. *Nature* 1986; 321: 168–171.